

# The global warming hiatus—a natural product of interactions of a secular warming trend and a multi-decadal oscillation

Shuai-Lei Yao · Gang Huang · Ren-Guang Wu · Xia Qu

Received: 26 June 2014 / Accepted: 22 December 2014 / Published online: 9 January 2015  
© Springer-Verlag Wien 2015

**Abstract** The globally-averaged annual combined land and ocean surface temperature (GST) anomaly change features a slowdown in the rate of global warming in the mid-twentieth century and the beginning of the twenty-first century. Here, it is shown that the hiatus in the rate of global warming typically occurs when the internally generated cooling associated with the cool phase of the multi-decadal variability overcomes the secular warming from human-induced forcing. We provide compelling evidence that the global warming hiatus is a natural product of the interplays between a secular warming tendency due in a large part to the buildup of anthropogenic greenhouse gas concentrations, in particular CO<sub>2</sub> concentration, and internally generated cooling by a cool phase of a quasi-60-year oscillatory variability that is closely associated with the Atlantic multi-decadal oscillation (AMO) and the Pacific decadal oscillation (PDO). We further illuminate that the AMO can be considered as a useful indicator and the PDO can be implicated as a harbinger of variations in global annual average surface temperature on multi-decadal timescales. Our

results suggest that the recent observed hiatus in the rate of global warming will very likely extend for several more years due to the cooling phase of the quasi-60-year oscillatory variability superimposed on the secular warming trend.

## 1 Introduction

Since the industrial revolution, greenhouse gas concentration in the atmosphere has been continuously increasing, which has been considered as a cause for the centennial warming trend of globally averaged surface temperature, especially since 1950 (Meehl et al. 2007). However, the global annual mean surface temperature has shown an apparent flattening trend in the twenty-first century (Easterling and Wehner 2009; Foster and Rahmstorf 2011), which challenges the prevailing notion that human-induced external forcing leads to global warming.

A variety of relevant mechanisms has been proposed for the recent hiatus in the rate of global warming. Up to now, there exist two schools of primary thoughts. One suggests that the response to external forcing is a main cause for the recent slowdown of global warming. The predominant reason includes the minimum in the recent total solar irradiance around 2009 as the sunspot number shows a much smaller decrease and the 11-year sunspot cycle lasts a bit longer than usual (Fröhlich 2012). Furthermore, some studies point out that the dramatic increase in the “background” stratospheric aerosols since 2000 in the absence of major volcanic eruptions (Solomon et al. 2011) and the rapid growth in tropospheric short-lived sulfur aerosols between 1998 and 2008 (Kaufmann et al. 2011) also contribute to a slowdown in radiative forcing and partially offset anthropogenic global

S.-L. Yao · G. Huang (✉)

State Key Laboratory of Numerical Modeling for Atmospheric Sciences and Geophysical Fluid Dynamics, Institute of Atmospheric Physics, Chinese Academy of Sciences, Beijing 100029, China  
e-mail: hg@mail.iap.ac.cn

S.-L. Yao

University of Chinese Academy of Sciences, Beijing 100049, China

G. Huang

Collaborative Innovation Center on Forecast and Evaluation of Meteorological Disasters, Nanjing University of Information Science & Technology, Nanjing 210044, China

R.-G. Wu · X. Qu

Center for Monsoon System Research, Institute of Atmospheric Physics, Chinese Academy of Sciences, Beijing 100029, China

warming. In addition, a negative radiative forcing due to a significant decrease in the stratospheric water vapor concentration since 2000 plays a key role in slowing the increase in globally averaged surface temperature during 2000–2009 (Solomon et al. 2010). The other school of thought considers that the internally generated variability of the climate system is the cause of the hiatus in global warming, at least in part. For instance, empirical model analysis demonstrated that La Niña-related cooling had favored the recent hiatus through partially offsetting the greenhouse gas-induced warming (Lean and Rind 2009). Consistently, recent study implied that La Niña-like decadal cooling in the eastern equatorial Pacific had caused a remarkable flattening trend in global annual average temperature from 2002 to 2012 (Kosaka and Xie 2013). There are suggestions that significant heat has been taken up by the oceans, especially in the Pacific (Balmaseda et al. 2013; Watanabe et al. 2013), which is in close agreement with an analysis of a global coupled climate model that showed that the deep ocean heat had increased during the hiatus period (Meehl et al. 2011). Therefore, there is no consensus within the scientific community concerning reasons for the occurrence of the hiatus in global warming.

The purpose of this study was to examine the relative contributions of a secular warming trend and a multi-decadal variability to global warming hiatus. We aim to gain a better understanding of the following questions. First, is the hiatus in global warming a common occurrence? Second, what are the relative roles of human-induced external forcing and internally generated multi-decadal variability? Finally, what are precursor signal and indicator of the hiatus? Understanding these questions has important implications for projecting the hiatus.

The rest of the paper is arranged as follows. Section 2 describes the observational data sets and analysis methods used in this study. Section 3 provides results on the range of the hiatus in the rate of global warming, showing the contributions from the secular warming trend and the quasi-60-year oscillatory variability tied to internally generated variability of the climate system. It also demonstrates the role of human-induced external forcing and internally generated variability in the hiatus of global warming. Section 4 concludes with a summary of the main findings and a discussion of the results.

## 2 Materials and methods

### 2.1 Data sources

We obtained three observed global annual mean combined land and ocean surface temperature (GST) anomaly data sets for the period 1880–2012, including Hadley Centre–Climatic Research Unit Version 4 (HadCRUT4; Morice et al. 2012) with the base period 1961–1990 from the Hadley Centre/

Climate Research Unit gridded surface temperature data set 4, Merged Land–Ocean Surface Temperature Analysis (MLOST; Smith et al. 2008) relative to the base period 1971–2000 from National Oceanic and Atmospheric Administration National Climate Data Center Merged Land–Ocean Surface Temperature Analysis, and Goddard Institute of Space Studies (GISS; Hansen et al. 2010) based on the period 1951–1980 from National Aeronautics and Space Administration Goddard Institute of Space Studies Surface Temperature Analysis, respectively. The HadISST sea surface temperature (SST) data set (Rayner et al. 2003) was obtained during 1880–2012 from the Hadley Centre/Climate Research Unit in the UK. Global CO<sub>2</sub> concentrations as observed at Mauna Loa are available during 1958–2012.

We apply the complete ensemble empirical mode decomposition (CEEMD) (Torres et al. 2011) to the time series of GST anomalies to extract the multi-decadal variability (MDV) and the secular trend (ST), as defined by intrinsic mode function (IMF), natural amplitude-frequency-modulated oscillatory functions. The details of the CEEMD are further described below. Besides, the sum of the MDV and the ST used here is defined as MDV+ST. In order to assess the statistical significance of the MDV and the ST, we utilize a statistical method that considers the energy of an IMF as a function of mean period of the IMF, tested against white noise (Huang and Wu 2008).

The monthly global mean SST (taken here to be 60° S–60° N) were removed to separate the actual Atlantic multi-decadal oscillation (AMO) signal and the actual Pacific decadal oscillation (PDO) signal from any global warming signal that may be present in the data. The AMO index during 1880–2012 was calculated by averaging detrended annual mean SST anomalies over the North Atlantic region (0°–60° N, 80° W–0°). The PDO index during 1880–2012 was derived from the standardized leading PC for the first EOF of detrended SST anomalies in the North Pacific domain (20° N–70° N, 110° E–80° W). Subsequent AMO index and PDO index discussed in this study are given by smoothing from a low-pass symmetric filter with 13 total weights and a half-power point at 16-year periods, with the reflective end points (Trenberth and Shea 2006).

### 2.2 Complete ensemble empirical mode decomposition

Assuming that an original signal  $x(t)$  satisfies two basic conditions: (1) the number of extrema and the number of zero crossing are equal or different at most by one and (2) the mean value of the lower and upper envelop is zero everywhere; then it can be decomposed into a finite number of intrinsic mode functions (IMFs) or modes by empirical mode decomposition (EMD) (Huang et al. 1998).

If  $x[n]$  is the targeted data, each  $x^i[n]$  ( $i=1, \dots, I$ ) is decomposed independently from the other realizations and

so for each one, a residue  $r_k^i[n]=r_{k-1}^i[n]-\text{IMF}_k^i[n]$  (1) can be obtained. Here, the decomposition modes will be defined as  $\overline{\text{IMF}}_k$ , then the first residue is calculated as  $r_1[n]=x[n]-\overline{\text{IMF}}_1[n]$  (2). We further compute the first EMD mode over an ensemble of  $r_1[n]$  plus different realizations of a given noise obtaining  $\overline{\text{IMF}}_2$  by averaging. The second residue is defined as  $r_2[n]=r_1[n]-\overline{\text{IMF}}_2[n]$  (3). This procedure will continue with the rest of the modes until the stopping criterion is reached.

We define the operator  $E_j(\cdot)$  which produces the  $j$ th mode obtained by EMD when giving a signal  $x[n]$ . Also, let us consider  $w^j$  as white noise with  $N(0,1)$ . The CEEMD algorithm can be described as:

1. Apply EMD to decompose  $I$  realizations  $x[n]+\varepsilon_0\omega^j[n]$  to obtain their first modes:

$$\overline{\text{IMF}}_1[n] = \frac{1}{I} \sum_{i=1}^I \text{IMF}_1^i[n]$$

2. Use Eq. (2) to calculate the first residue at the first stage ( $k=1$ ).

$$r_1[n] = x[n]-\overline{\text{IMF}}_1[n]$$

3. Continue to decompose realizations  $r_1[n]+\varepsilon_1E_1(\omega^j[n])$ ,  $i=1, \dots, I$ , until their first EMD and calculate the second mode as

$$\overline{\text{IMF}}_2[n] = \frac{1}{I} \sum_{i=1}^I E_1(r_1[n] + \varepsilon_1E_1(\omega^j[n]))$$

4. For  $k=2, \dots, K$ , calculate the  $k$ th residue as

$$r_k[n] = r_{(k-1)}[n]-\overline{\text{IMF}}_k[n]$$

5. Continue to decompose realizations  $r_k[n]+\varepsilon_kE_k(\omega^j[n])$ ,  $i=1, \dots, I$ , until their first EMD and calculate the  $(k+1)$ -th mode as

$$\overline{\text{IMF}}_{k+1}[n] = \frac{1}{I} \sum_{i=1}^I E_1(r_k[n] + \varepsilon_kE_k(\omega^j[n]))$$

6. Go back to step 4 for the next  $k$ .

Steps 4 to 6 are continually performed until the obtained residue does not have at least two extrema and is no longer to

be decomposed. The final residue can be defined as

$$R[n] = x[n]-\sum_{k=1}^K \overline{\text{IMF}}_k,$$

with  $K$  as the total number of modes. Thus, the original given signal  $x[n]$  can be defined as

$$x[n] = \sum_{k=1}^K \overline{\text{IMF}}_k + R[n]$$

In this study, considering that the observed global annual mean surface temperature anomaly data sets are obtained from combined land and ocean surface temperature, noise standard deviation of  $\varepsilon=0.3$ , and an ensemble size of  $I=1000$  are used (Huang and Wu 2008).

### 2.3 Statistical test analysis

Here, we assume that the time series used in this study are quasi-stationary when testing a sample correlation between two auto-correlated time series  $X$  and  $Y$  at a given lag  $k$ , denoted  $r_{XY}(k)$ . Meanwhile, we assume a null hypothesis of no correlation at all given lags. The effective number of degrees of freedom,  $N^{\text{eff}}$  of  $r_{XY}(k)$  for the time series  $X$  and  $Y$  is estimated using the modified Chelton method (Li et al. 2012; Pyper and Peterman 1998) in order to test the significance of the correlation between two auto-correlated time series.  $N^{\text{eff}}$  is calculated by the following theoretical approximation:

$$\frac{1}{N^{\text{eff}}} \approx \frac{1}{N} + \frac{2}{N} \sum_{j=1}^N \frac{N-j}{N} \rho_{XX}(j)\rho_{YY}(j), \tag{1}$$

where  $N$  is the sample size and  $\rho_{XX}(j)$  and  $\rho_{YY}(j)$  are the autocorrelations of two sampled time series  $X$  and  $Y$  at time lag  $j$ , respectively. Given  $N^{\text{eff}}$ , the standard critical value for  $r_{XY}(k)$  at the  $\alpha$  significance level can be obtained from the  $t$  distribution for either one- or two-tailed tests. The solution is as follows:

$$r_{\text{crit}} = \sqrt{t_{\alpha, N^{\text{eff}}}^2 / (t_{\alpha, N^{\text{eff}}}^2 + N^{\text{eff}})}. \tag{2}$$

When  $r_{XY}(k)$  is bigger than  $r_{\text{crit}}$ , the correlation between two sampled time series  $X$  and  $Y$  at a lag  $k$  is considered highly significant at the  $\alpha$  level.

### 3 Results

#### 3.1 Statistical significance test of MDV and ST

In Fig. 1, we use the CEEMD to decompose the observed global mean surface temperature (GST) anomalies, combined land and ocean time series derived from HadCRUT4, GISS, and MLOST data sets, which cover the period of 1880

through 2012. As can be seen, the GST anomaly time series from all the three datasets are decomposed into seven IMFs. The IMF modes exhibit oscillatory behavior with varying amplitudes and frequencies. The first three IMFs (IMF1, IMF2, and IMF3) contain high-frequency information on inter-annual timescales (less than 10 years). The fourth IMF (IMF4) corresponds to decadal timescales with a mean period of 13 years. And the fifth IMF (IMF5) corresponds to decadal

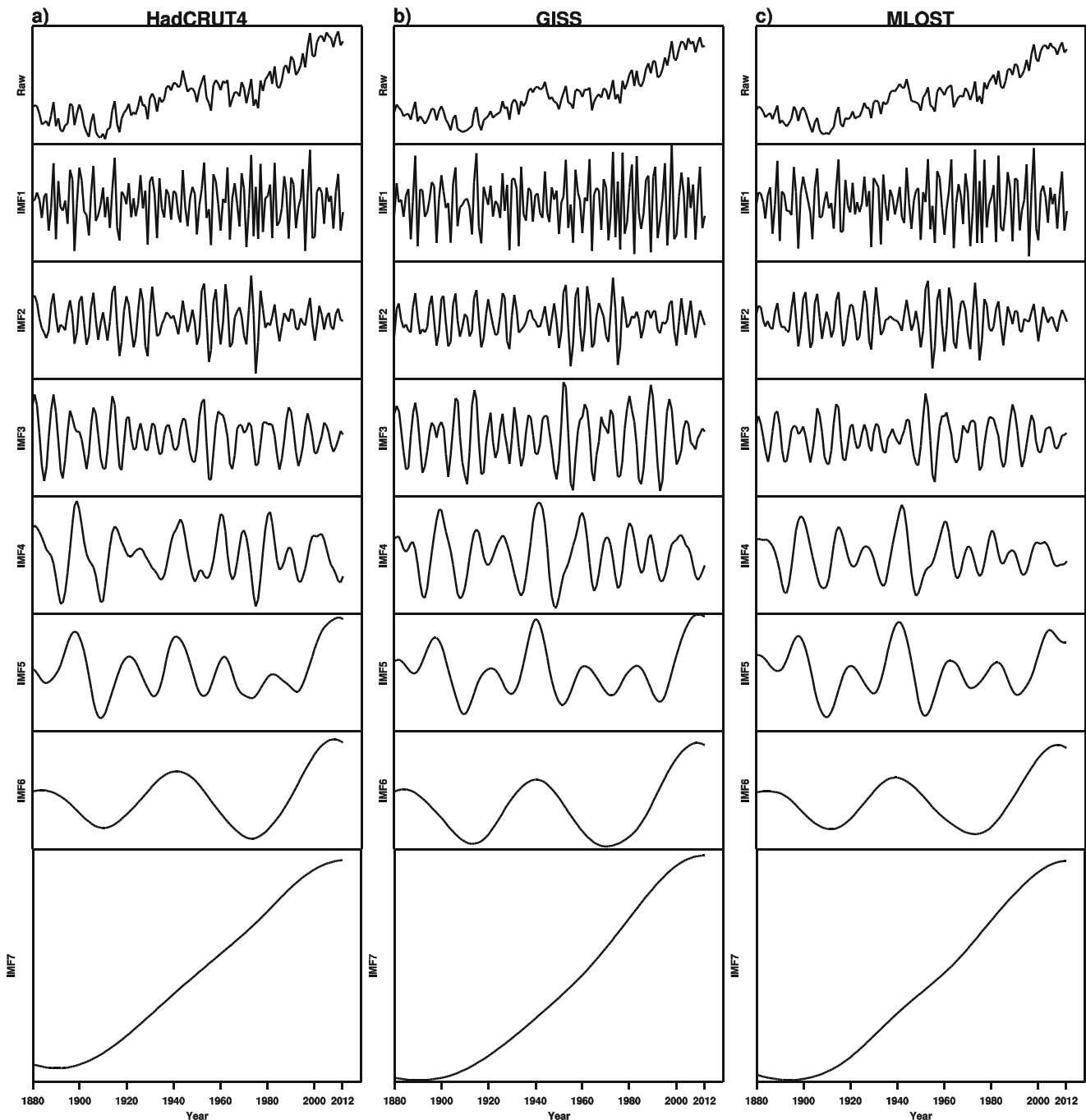


**Fig. 1** CEEMD decompositions of the time series of observed global annual mean combined land and ocean surface temperature anomalies for the period 1880–2012. In each panel, the *top black curve* shows the

raw time series and the next *seven black curves* represent CEEMD components ( $IMF_j, j=1, \dots, 7$ ) from high frequency to low frequency. **a, b, c** for HadCRUT4, GISS, and MLOST, respectively

to inter-decadal timescales with a mean period of 24 years. In addition, the sixth IMF (IMF6) approaches multi-decadal timescales with a mean period of quasi-60 years, and the seventh IMF (IMF7) represents a monotonically increasing function of time that seems to be trend-like in nature. Here, the characteristics of interest in this study get involved in the IMF6 and IMF7, which are referred to as MDV and ST, respectively.

To determine whether or not the MDV and ST time series recovered from the GST anomaly time series containing significant signals that can be distinguished from background noise of the climate system, we investigate statistical significance of the MDV and ST time series extracted using an adaptive method such as the CEEMD. In Fig. 2, we evaluate the statistical significance of the MDV and ST time series. The MDV and the ST time series from GST anomalies time series (based on all the three data sets used here) are shown to be evidently distinguishable from white noise at above the 99 % confidence level and are in this sense statistically significant with reference to the white noise null hypothesis (Fig. 2). This provides a strong evidence of the statistical significance of the MDV and ST time series extracted from the CEEMD. Our results constitute proof that the MDV and ST obtained here can be considered as distinct from stochastically forced climate variability driven by weather noise (white noise). Meanwhile, it also demonstrates that the MDV and ST time series derived from GST anomaly time series are not sensitive to different observational data sets and hold indeed important climate signals that can be separated from background noise.

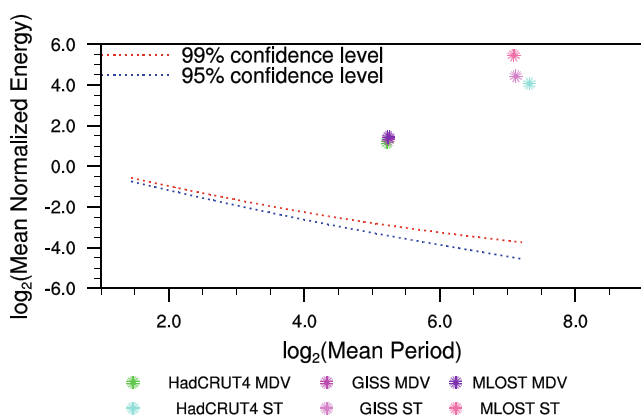
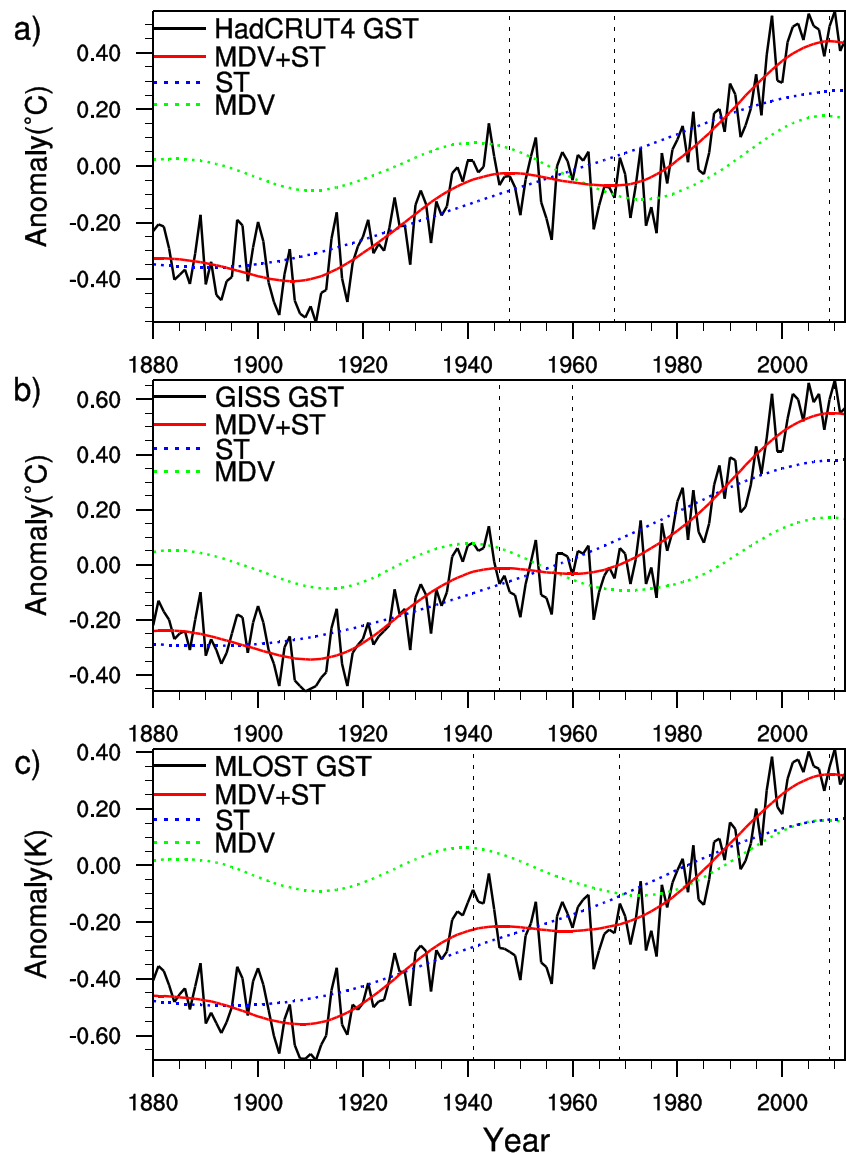


**Fig. 2** Statistical significance test of the MDV and ST time series from GST anomaly time series for HadCRUT4, GISS, and MLOST, respectively, against white noise null hypotheses. The *dots* indicate the MDV and ST time series from different data sets by different colors. Each *sign* denotes the mean normalized energy of the MDV (ST) as a function of mean period of the MDV (ST). The *red dashed line* and the *blue dashed line* illustrate the 99th and 95th percentiles of noise intrinsic model function mean normalized energy distribution as a function of mean period, respectively. Any *sign* (the MDV or ST) that stays above the red dashed line is referred to as statistically significant at the 99 % confidence level

### 3.2 The hiatus in global warming

The time series of GST anomalies, MDV+ST, ST, and MDV during 1880–2012 from HadCRUT4, GISS, and MLOST, respectively, are shown in Fig. 3. It can be seen that all the time series of GST anomalies (Fig. 3, black solid line) and MDV (Fig. 3, green dashed line) from three data sets exhibit an obvious warming-cooling-warming (WCW) pattern (Thompson et al. 2010) in the twentieth century and a recent slowdown in the globally averaged annual surface temperature warming trend (Swanson and Tsonis 2009). Specifically, all the time series of MDV display a multi-decadal oscillatory variability, marked by a clear quasi-60-year long cycle. It is likely that oceanic modes of multi-decadal oscillatory variability play a prominent role in causing the MDV. And all the time series of ST (Fig. 3, blue dashed line) reveal a nearly monotonic warming trend, which to a large part coincides with the increase rate of global warming due to the buildup of greenhouse gas concentrations. It is also noted that all the time series of MDV+ST (Fig. 3, red solid line) superimposed on the GST anomaly time series show a marked WCW-like pattern in the twentieth century. In addition, the MDV+ST time series are characterized by a hiatus in the mid-twentieth century and a recent slowdown of global warming. For example, HadCRUT4 MDV+ST (Fig. 3a) has a slope of  $-0.0021$  °C/year from 1948 to 1968 and has a trend of cooling  $0.0016$  °C/year during 2009–2012. GISS MDV+ST (Fig. 3b) displays a decreasing trend of  $-0.0014$  °C/year from 1946 to 1960 and  $-0.0387$  °C/year over the years 2010–2012. For MLOST (Fig. 3c), a trend of cooling of  $0.0003$  °C/year is seen from 1941 to 1969 and a slope of  $-0.0014$  °C/year is observed during 2009–2012. It should be noted that observed SST datasets had sparse coverage for the period during and shortly after World War II (Chowdary et al. 2012; Izumo et al. 2014; Thompson et al. 2008) because SST datasets were sampled on board ships based on various measurement techniques, including measurements taken from insulated and uninsulated buckets (UK ships) and engine room intake (US ships). In order to reduce observational uncertainty due to sampling errors, the quality control has been used to reconstruct global mean combined land and ocean surface temperature datasets. Additionally, the three datasets have been successfully employed to monitor the Earth's climate in the Intergovernmental Panel on Climate Change Fifth Assessment Report. Thus, our results discussed in this study, in some sense, are qualitatively unaffected by the data gap during World War II and a few years thereafter. The results above are suggestive of a common hiatus in the rate of global warming. The hiatus phenomenon typically occurs when a cooling contribution from a quasi-60-year multi-decadal oscillation overwhelms the long-term warming trend from external forcing. Our results also suggest that global warming hiatus may be a natural product of the interplay between a long-term warming trend

**Fig. 3** Shown are GST anomalies, MDV+ST, ST, and MDV time series from 1880 to 2012. **a** For HadCRUT4, the *black solid line* indicates the GST anomaly time series; the *red solid line* shows the MDV+ST time series; the *blue dashed line* denotes the ST time series; the *green dashed line* represents the MDV time series; *black vertical dashed lines* are shown to mark the MDV+ST polarity reversal times in 1947, 1969, and 2009. **b** Same as **a** but for GISS (polarity reversal times in 1946, 1961, and 2009). **c** Same as **a** but for MLOST (polarity reversal times in 1940, 1970, and 2009)



and a cooling phase of a multi-decadal oscillatory variability (quasi-60-year period), as evidenced by the qualitatively similar results (Wu et al. 2011).

### 3.3 Human-induced external forcing and internally generated variability

Results of climate model simulations have shown that the MDV is a natural mode of internally generated variability of the climate system, originating primarily from changes in oceanic circulation, for example, the dominant internal multi-decadal variability related to the Atlantic multi-decadal oscillation (AMO) in the North Atlantic is characterized by sea surface temperature anomalies of the same sign from the equator to the high latitudes, with some cooling in the subpolar regions of the North Atlantic (Latif et al. 2004), and the predominant intrinsic inter-decadal variability tied to the Pacific

decadal oscillation (PDO) in the North Pacific is characteristic of the warm phase with cooling in the central North Pacific and warming along with the west coast of the Americas, and the cool phase opposite of the warm phase (Mantua and Hare 2002). Also, the ST is largely caused by the response to the buildup of anthropogenic greenhouse gas concentrations (Swanson et al. 2009). In order to capture some implications of the physical processes that may contribute to the MDV and the ST, we regressed the global annual sea surface temperature (SST) anomaly field onto the standardized MDV and ST time series for the period 1880–2012. Regression maps for HadCRUT4, GISS, and MLOST are displayed in Fig. 4. Paramount signals in the regression pattern for the MDV are restricted to the North Atlantic region and the North Pacific sector, especially over the extratropical North Atlantic, the west coast of the North America, and the east coast of East Asia with positive regression coefficients (Fig. 4a, c, e). Our

research has identified compelling evidence that the Pacific decadal timescale variations may be specifically tied to climate change related to global warming (Trenberth and Hurrell 1994), and the North Atlantic-Arctic sector could have considerably contributed to a hemispheric and even a global scale surface air temperature response to multi-decadal timescale surface flux anomalies simulated by climate model experiments (Semenov et al. 2010). Both observations (Polyakov et al. 2010) and climate model simulations (Knight et al. 2005) imply that episodes of rising and falling SST over the North Atlantic are associated with variations in the intensity of the thermohaline circulation, as inferred from the SST pattern for the MDV depicted in Fig. 4a, c, e. The regression pattern for the ST in Fig. 4b, d, f shows worldwide warming except for some patched areas where slight cooling has appeared, e.g., parts of the Southern Ocean, parts of equatorial central and eastern Pacific, and the northwestern North Atlantic

Ocean, which is due in large part to the response to anthropogenic forcing over the most of global oceans (Ting et al. 2009). Our results in Fig. 4 and the statistical analysis of CMIP3 control runs and forced runs (DelSole et al. 2011) highlight that the ST is largely caused by human-induced external forcing, particularly CO<sub>2</sub>, and the MDV mostly arises from internally generated multi-decadal variability of the climate system, simultaneously with the ST. Additionally, these results lend credence to the view that the ST and the MDV may be meaningful for representing the anthropogenic and internal components of GST on multi-decadal timescales.

Previous observational and modeling studies have shown that there exists an apparent linkage between a multi-decadal oscillation in the North Atlantic (a AMO-like mode) and eastern North Pacific non-ENSO sea surface temperature anomaly variability (a PDO-like mode) (Mestas-Nuñez and Enfield 1999). Enfield et al. (2001) also reported that the correlations

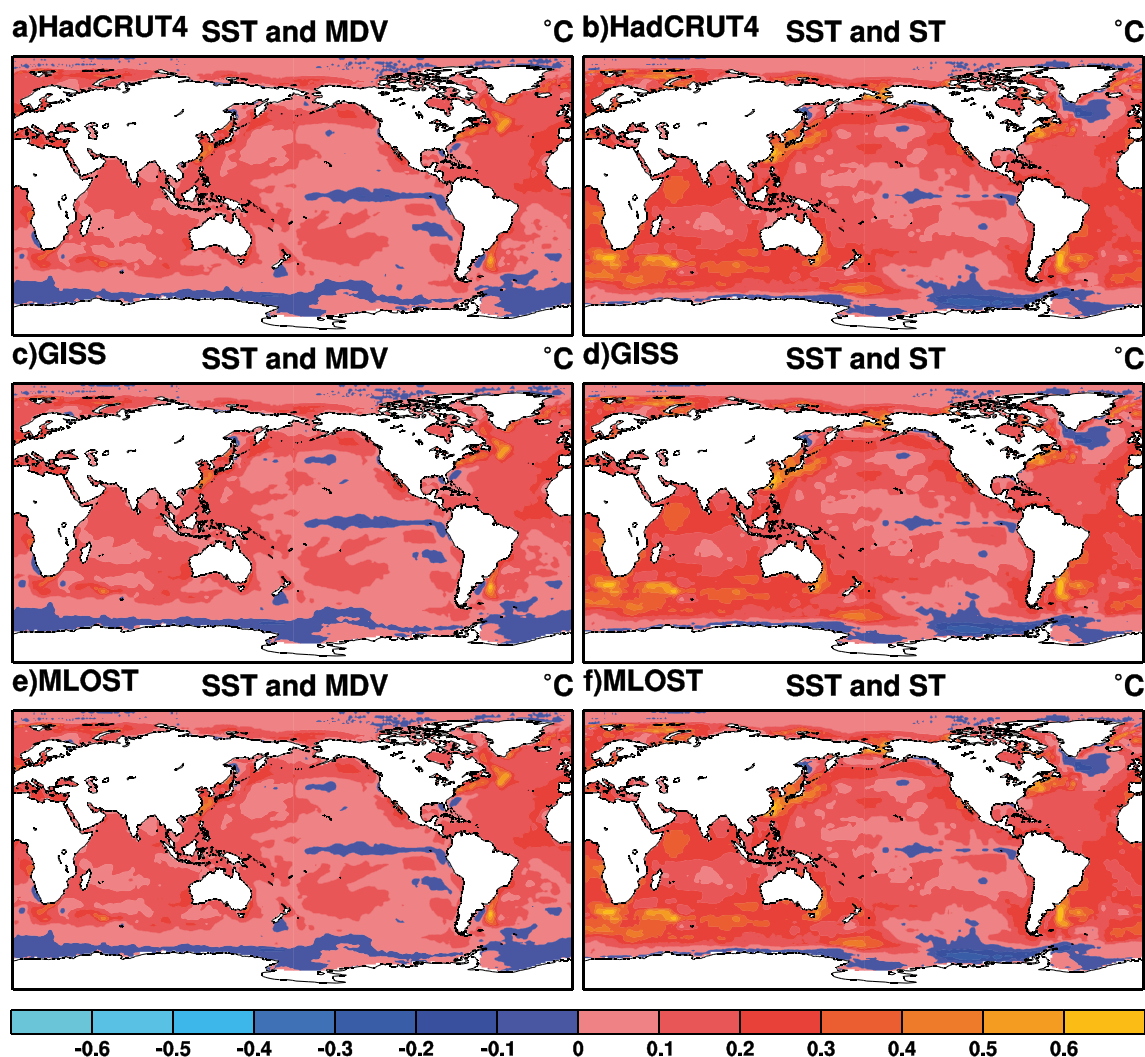


**Fig. 4** Regressions of global annual sea surface temperature (SST) anomalies for 1880–2012 with standardized time series of the MDV and ST. **a, c, e** Global annual SST anomalies regressed onto the standardized MDV time series from HadCRUT4, GISS, and MLOST,

respectively. **b, d, f** Global annual SST anomalies regressed onto the standardized ST time series from HadCRUT4, GISS, and MLOST, respectively. The annual SST anomalies are calculated as departure from the 1961–1990 climatology

between the AMO index and sea surface temperature anomaly in the Pacific, especially of 40° N, were high, and the sea surface temperature anomaly signal may enhance the multi-decadal oscillation mode in the North Atlantic. Guan and Nigam (2009) further highlighted that a considerable portion of the North Atlantic multi-decadal variability stemmed from the Pacific links. Regression pattern of annual SST anomalies on the AMO index (Fig. 5a) suggests some significant connection between the AMO and SST anomalies in Southern Ocean and the North Pacific SST variability (Ting et al. 2009). In addition, the PDO mode also reveals surprising connections to the North Atlantic, with high correlations resembling the AMO mode (Fig. 5b), as confirmed in previous study (Guan and Nigam 2008). To some extent, it is argued that an atmospheric teleconnection between the North Atlantic and the North Pacific plays a key role in mediating the relationship between the AMO and the PDO (Trenberth et al. 2014), for example, through AO/NAO. Determining the nature and realism of the AMO and the PDO in coupled ocean-

atmosphere models is a crucial next step leading to a better understanding of the relationship between the AMO mode and the PDO mode. Further work on the AMO and the PDO dynamics and their predictability is warranted.

To further substantiate the close relationship between the ST and CO<sub>2</sub> concentrations, as well as the MDV and the PDO, and the AMO, respectively, we compare time series of the ST and CO<sub>2</sub> concentrations, the MDV and the PDO index, and the AMO index in Fig. 6. It is clear that the ST and the MDV exhibit some slight differences in amplitude and shape during 1880–2012 in Fig. 6a, b, c in large part because different data products and different methods have been applied to homogenize surface air temperature over land and sea surface temperature over ocean. Fortunately, it is not likely to qualitatively influence the results that we present in this study. The ST and CO<sub>2</sub> concentrations display a strong upward trend from 1958 onward (Fig. 6a), implying that the buildup of anthropogenic greenhouse gas concentrations projects largely on the ST, as shown in Fig. 4b, d, f. Moreover, it is obvious from

**Fig. 5** a Regression pattern of global annual sea surface temperature (SST) anomalies (the global mean SST anomaly removed) on standardized time series of the annual mean AMO index, based on the HadISST data set for the period 1880–2012. b Same as a but for the annual mean PDO index

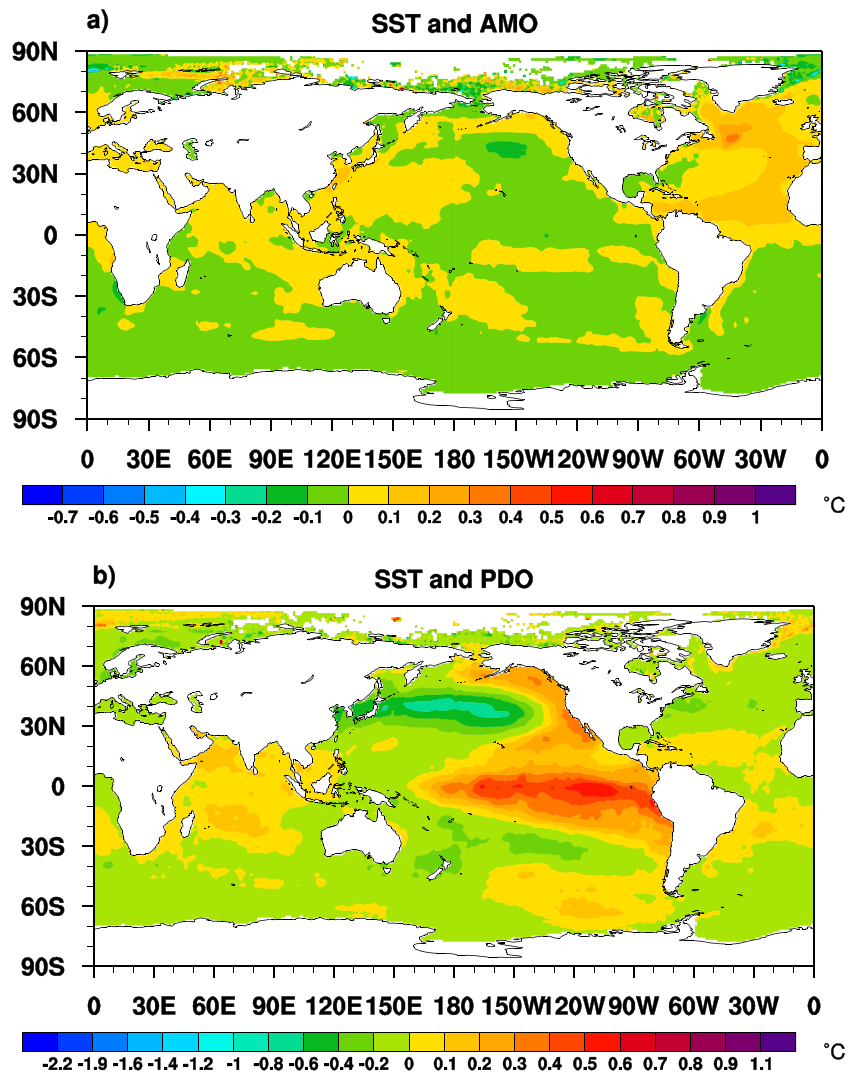




**Fig. 6** CO<sub>2</sub> concentrations from 1858 to 2012, the MDV, the ST, and smoothed annual mean PDO and AMO indices during 1880–2012. **a** Time series of the ST from HadCRUT4 (navy blue solid line), GISS (magenta solid line), and MLOST (green solid line), respectively. The red solid line denotes observed atmospheric CO<sub>2</sub> concentration time series ( $\times 10^2$  ppmv) in the Manua Loa. **b** Time series of the MDV from HadCRUT4 (navy blue solid line), GISS (magenta solid line), and MLOST (green solid line), respectively. The red solid line shows the annual mean PDO index. **c** Same as **b** except that the red solid line represents the annual mean AMO index (°C)

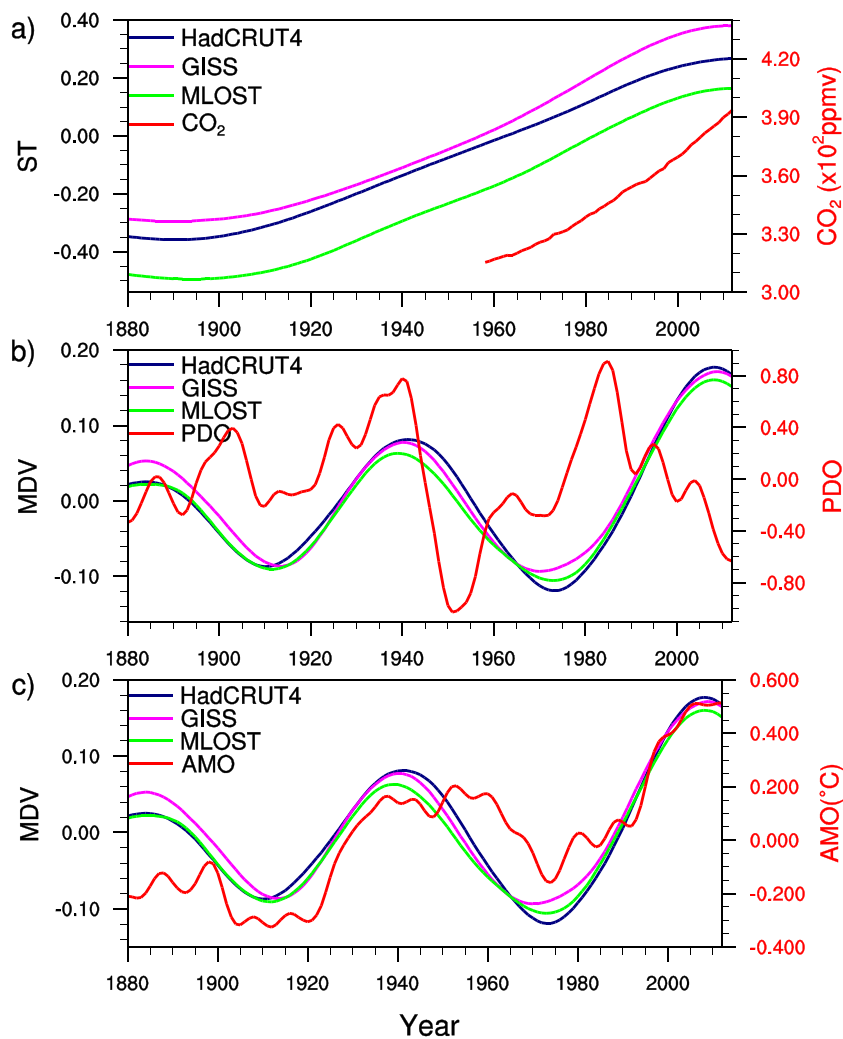
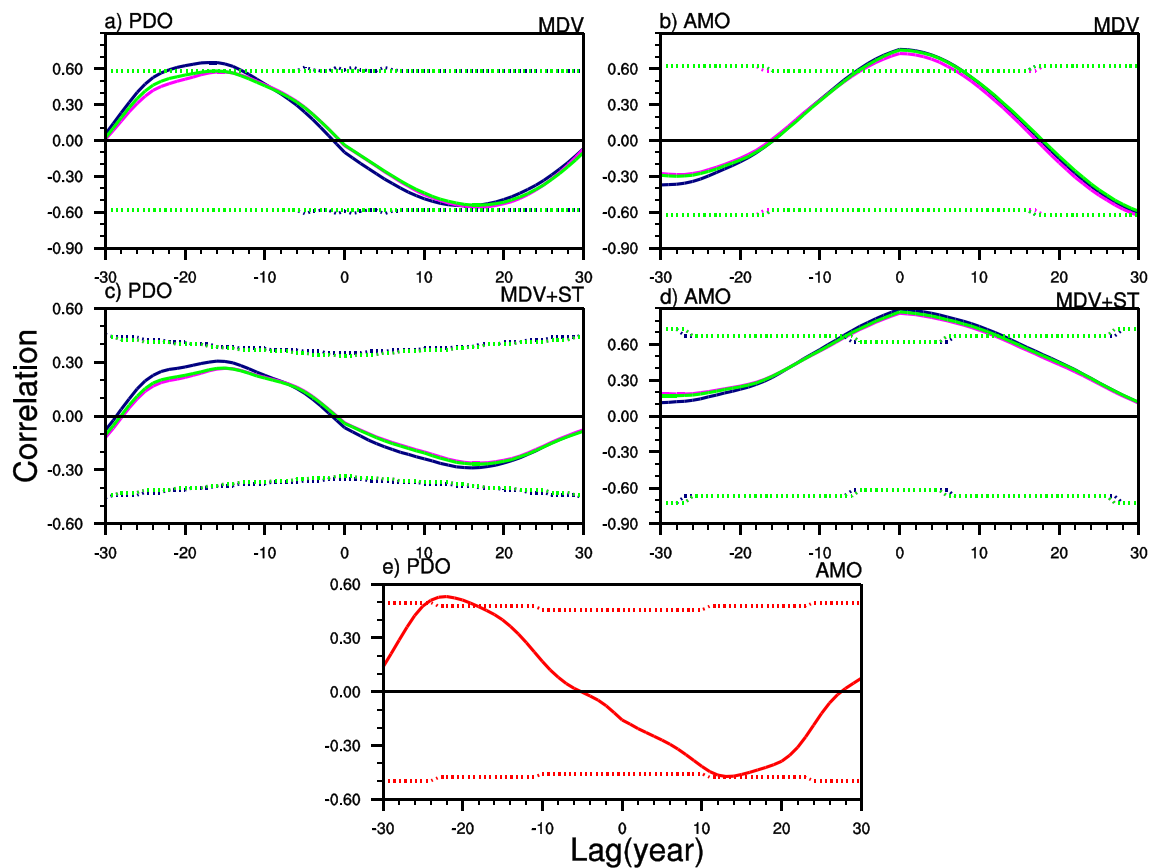


Fig. 6b that the annual mean PDO index and the MDV show a phase lag of about 10–20 years (the PDO index leading the MDV time series). As shown in Fig. 7a, the maximum positive correlation coefficients (all exceeding 0.58, although slightly different for each of the MDV time series, significant at the 90 % confidence level) occur at a lead of approximately 16 years (the PDO index leading the MDV time series). The simultaneous correlation coefficients are near zero (Fig. 7a). Meanwhile, it is also notable that the multi-decadal fluctuations of annual mean AMO index appear to be largely in phase with those of the MDV time series (Fig. 6c). As is evident in Fig. 7b, the maximum correlation coefficients (all exceeding 0.73, significant at the 90 % confidence level) are observed between the AMO index and the MDV time series at zero lag, and no significant correlations are found when the AMO index leads (lags) the MDV time series. As the MDV is largely a reflection of internally generated multi-decadal variability of the climate system associated with the PDO and the AMO, our study implies that global warming hiatus is largely a natural product of interactions of a long-term warming contribution

from the increase of anthropogenic greenhouse gas concentrations and the cooling phase of quasi-60-year oscillation connected with the AMO and the PDO. The occurrences of the hiatus in the rate of global warming typically occur when the secular warming from human-induced forcing are overwhelmed by internally generated cooling associated with the AMO and the PDO.

### 3.4 The harbinger and indicator of the hiatus phenomenon

In the following, we will focus on the close link between the GST anomalies and the PDO index, and the AMO index, respectively. The impact of the AMO on surface air temperature over much of the globe has been studied extensively in observations and numerical simulations (Zhang et al. 2007). And the PDO also has an indirect influence on continental and global surface air temperature (Mantua et al. 1997). As seen in Fig. 7c, the correlations between the annual mean PDO index and the MDV+ST time series are explicitly positive (approximately 0.30, although not significant at 90 % confidence



**Fig. 7** **a** Lead-lagged correlation between the annual mean PDO index and the MDV time series during 1880–2012 for HadCRUT4 (navy blue solid line), GISS (magenta solid line), and MLOST (green solid line). Negative (positive) lags mean that the annual mean PDO index leads (lags) the MDV time series. The navy blue, magenta, and green dashed lines denote the 90 % confidence levels for HadCRUT4, GISS, and MLOST, respectively, using the effective number of degrees of freedom.

**b** Same as **a** but for the annual mean AMO index and the ST time series. **c** Same as in **a** but for the annual mean PDO index and the MDV+ST time series. **d** Same as **c** but for the annual mean AMO index and the MDV+ST time series. **e** Lead-lagged correlation between the annual mean PDO and AMO index during 1880–2012 (red solid line). The red dashed line denotes the 90 % confidence level

level) when the PDO index leads the MDV+ST time series by around 16 years, which is in close agreement with the lead correlations between the PDO index and the MDV time series (Fig. 7a). On the other hand, the most significant positive correlations (exceeding 0.86, at 90 % confidence level) are found between the annual mean AMO index and the MDV+ST time series at lag zero (Fig. 7d). In addition, the PDO and the AMO are not completely independent, and they may have unassailable relevance via an atmospheric bridge or remote forcing, as discussed in Fig. 5. High correlation coefficients (approximately 0.53, significant at 90 % confidence level) are obtained between the annual mean PDO index and the annual mean AMO index at about 22-year lead (Fig. 7e). The 16-year lead of the PDO index compared to the MDV+ST time series implies that it can be regarded as a useful harbinger of concurrence of a secular warming trend and a quasi-60-year period multi-decadal oscillatory variation. Likewise, a coincidence of the annual mean AMO index and the MDV+ST time series suggests that the AMO can be considered as an instantaneous indicator of variations of GST anomalies on multi-

decadal timescales. These results provide further evidence that we can use the PDO and AMO signal to give an advance projection of the multi-decadal oscillatory variation of GST anomalies by establishing a dynamical model with relevant physical interpretations. According to the quasi-60-year period oscillation superimposed on the ST, our results suggest that there is a chance that the recent observed slowdown in the rate of global warming could potentially continue and it is very likely that the recent hiatus will extend for several more years. Similar projection that the recent observed hiatus of North Hemisphere tends to last until 2027 has been verified (Li et al. 2013). The projection will need to be further investigated by climate dynamic model.

#### 4 Conclusions and discussions

Our results demonstrate that the observed globally averaged annual combined land and ocean surface temperature

anomalies have stayed flat in the mid-twentieth century and the beginning of the twenty-first century by examining time series of the MDV, the ST, and the MDV+ST recovered from CEEMD of GST anomalies from HadCRUT4, GISS, and MLOST during 1880–2012. Furthermore, it is shown that the occurrences of the hiatus in the rate of global warming are a natural product of the interplay between a secular warming contribution from the buildup of anthropogenic greenhouse gas concentrations and the unprecedented cooling phase of a quasi-60-year cycle multi-decadal oscillatory variation associated with the AMO and the PDO. The ST is predominantly caused by the increasing anthropogenic greenhouse gas concentrations, especially CO<sub>2</sub> concentrations, and the MDV is in large part due to internally generated multi-decadal variability of the climate system associated with the AMO and the PDO. Our results reveal that the PDO index leads the MDV+ST time series by around 16 years, and the AMO index is almost in phase with the MDV+ST time series. These results also highlight that the PDO can be served as a useful precursor signal in the projected variations of GST anomalies on multi-decadal timescales. Meanwhile, the AMO can be used as an implemental indicator of the multi-decadal oscillatory variation of GST anomalies. Our study suggests that there is a chance that the recent observed hiatus could potentially continue, and it is very likely that the current observed slowdown in the rate of global warming will extend for several more years, as indicated by the maintained cooling phase of the MDV+ST from HadCRUT4, MLOST, and GISS.

Some limitations of our results should be acknowledged. Firstly, the nature of the interplay between human-induced external forcing and internally generated multi-decadal variability associated with the AMO and the PDO should deserve more explicit considerations. Secondly, the associated physical interpretations underlying the influence of the PDO and the AMO on the multi-decadal oscillatory variations of GST anomalies remain unclear. Finally, how to establish a scientific climate dynamical model for projecting the current hiatus duration in global warming needs to be further investigated. Future work of understanding the mechanisms, predictability, and climate impacts of the AMO and the PDO is instrumental for better modeling and future projection of global climate change on multi-decadal timescales.

**Acknowledgments** We thank Weichen Tao, Guanjuan Wen, and Hainan Gong for the useful discussions and suggestions for this work. Thanks are also due to Shangfeng Chen and Dong Chen for their comments on a previous version of the manuscript. This work is supported by the National Basic Research Program of China (2012CB955604 and 2011CB309704), the Strategic Priority Research Program of the Chinese Academy of Sciences (XDA05090402), the National Natural Science Foundation of China (41275083 and 91337105), and National Outstanding Youth Science Fund Project of China (41425019).

## References

- Balmaseda MA, Trenberth KE, Källén E (2013) Distinctive climate signals in reanalysis of global ocean heat content. *Geophys Res Lett* 40: 1754–1759
- Chowdary J, Xie S-P, Tokinaga H, Okumura YM, Kubota H, Johnson N, Zheng X-T (2012) Interdecadal variations in ENSO teleconnection to the Indo-Western Pacific for 1870–2007\*. *J Climate* 25:1722–1744
- DelSole T, Tippett MK, Shukla J (2011) A significant component of unforced multidecadal variability in the recent acceleration of global warming. *J Climate* 24:909–926
- Easterling DR, Wehner MF (2009) Is the climate warming or cooling? *Geophys Res Lett* 36(8):19440–8007
- Enfield DB, Mestas-Nuñez AM, Trimble PJ (2001) The Atlantic multidecadal oscillation and its relation to rainfall and river flows in the continental. *US Geophys Res Lett* 28:2077–2080
- Foster G, Rahmstorf S (2011) Global temperature evolution 1979–2010. *Environ Res Lett* 6:044022
- Fröhlich C (2012) Total solar irradiance observations. *Surv Geophys* 33: 453–473
- Guan B, Nigam S (2008) Pacific sea surface temperatures in the twentieth century: an evolution-centric analysis of variability and trend. *J Climate* 21:2790–2809
- Guan B, Nigam S (2009) Analysis of Atlantic SST variability factoring interbasin links and the secular trend: clarified structure of the Atlantic multidecadal oscillation. *J Climate* 22:4228–4240
- Hansen J, Ruedy R, Sato M, Lo K (2010) Global surface temperature change. *Rev Geophys* 48:RG4004
- Huang NE, Wu Z (2008) A review on Hilbert-Huang transform: method and its applications to geophysical studies. *Rev Geophys* 46: RG2006
- Huang NE et al (1998) The empirical mode decomposition and the Hilbert spectrum for nonlinear and non-stationary time series analysis. *Proc Roy Soc Lond Math Phys Eng Sci* 454:903–995
- Izumo T, Lengaigne M, Vialard J, Luo J-J, Yamagata T, Madec G (2014) Influence of Indian Ocean dipole and Pacific recharge on following year's El Niño: interdecadal robustness. *Clim Dyn* 42:291–310
- Kaufmann RK, Kauppi H, Mann ML, Stock JH (2011) Reconciling anthropogenic climate change with observed temperature 1998–2008. *Proc Natl Acad Sci* 108:11790–11793
- Knight JR, Allan RJ, Folland CK, Vellinga M, Mann ME (2005) A signature of persistent natural thermohaline circulation cycles in observed climate. *Geophys Res Lett* 32(20):1944–8007
- Kosaka Y, Xie S-P (2013) Recent global-warming hiatus tied to equatorial Pacific surface cooling. *Nature* 501:403–407. doi:10.1038/nature12534
- Latif M et al (2004) Reconstructing, monitoring, and predicting multidecadal-scale changes in the North Atlantic thermohaline circulation with sea surface temperature. *J Climate* 17:1605–1614
- Lean JL, Rind DH (2009) How will Earth's surface temperature change in future decades? *Geophys Res Lett* 36:L15708
- Li Y, Li J, Feng J (2012) A teleconnection between the reduction of rainfall in Southwest Western Australia and North China. *J Clim* 25:8444–8461
- Li J, Sun C, Jin FF (2013) NAO implicated as a predictor of Northern Hemisphere mean temperature multidecadal variability. *Geophys Res Lett* 40:5497–5502
- Mantua NJ, Hare SR (2002) The Pacific decadal oscillation. *J Oceanogr* 58:35–44
- Mantua NJ, Hare SR, Zhang Y, Wallace JM, Francis RC (1997) A Pacific interdecadal climate oscillation with impacts on salmon production. *Bull Am Meteorol Soc* 78:1069–1079

- Meehl G et al. (2007) Climate change 2007: the physical science basis contribution of working group I to the fourth assessment report of the intergovernmental panel on climate change:747–846
- Meehl GA, Arblaster JM, Fasullo JT, Hu A, Trenberth KE (2011) Model-based evidence of deep-ocean heat uptake during surface-temperature hiatus periods. *Nat Clim Chang* 1:360–364
- Mestas-Núñez AM, Enfield DB (1999) Rotated global modes of non-ENSO sea surface temperature variability. *J Climate* 12:2734–2746
- Morice CP, Kennedy JJ, Rayner NA, Jones PD (2012) Quantifying uncertainties in global and regional temperature change using an ensemble of observational estimates: the HadCRUT4 data set. *J Geophys Res: Atmospheres* (1984–2012), 117(D8):2156–2202
- Polyakov IV, Alexeev VA, Bhatt US, Polyakova EI, Zhang X (2010) North Atlantic warming: patterns of long-term trend and multidecadal variability. *Clim Dyn* 34:439–457
- Pyper BJ, Peterman RM (1998) Comparison of methods to account for autocorrelation in correlation analyses of fish data. *Can J Fish Aquat Sci* 55:2127–2140
- Rayner N et al. (2003) Global analyses of sea surface temperature, sea ice, and night marine air temperature since the late nineteenth century. *J Geophys Res: Atmospheres* (1984–2012), 108(D14):2156–2202
- Semenov VA, Latif M, Dommenges D, Keenlyside NS, Strehz A, Martin T, Park W (2010) The impact of North Atlantic-Arctic multidecadal variability on Northern Hemisphere surface air temperature. *J Climate* 23:5668–5677
- Smith TM, Reynolds RW, Peterson TC, Lawrimore J (2008) Improvements to NOAA's historical merged land-ocean surface temperature analysis (1880–2006). *J Climate* 21:2283–2296
- Solomon S, Rosenlof KH, Portmann RW, Daniel JS, Davis SM, Sanford TJ, Plattner G-K (2010) Contributions of stratospheric water vapor to decadal changes in the rate of global warming. *Science* 327:1219–1223
- Solomon S, Daniel J, Neely R, Vernier J-P, Dutton E, Thomason L (2011) The persistently variable “background” stratospheric aerosol layer and global climate change. *Science* 333:866–870
- Swanson KL, Tsonis AA (2009) Has the climate recently shifted? *Geophys Res Lett* 36(6):1944–8007
- Swanson KL, Sugihara G, Tsonis AA (2009) Long-term natural variability and 20th century climate change. *Proc Natl Acad Sci* 106:16120–16123
- Thompson DW, Kennedy JJ, Wallace JM, Jones PD (2008) A large discontinuity in the mid-twentieth century in observed global-mean surface temperature. *Nature* 453:646–649
- Thompson DW, Wallace JM, Kennedy JJ, Jones PD (2010) An abrupt drop in Northern Hemisphere sea surface temperature around 1970. *Nature* 467:444–447
- Ting M, Kushnir Y, Seager R, Li C (2009) Forced and internal twentieth-century SST Trends in the North Atlantic\*. *J Climate* 22:1469–1481
- Torres ME, Colominas MA, Schlotthauer G, Flandrin P (2011) A complete ensemble empirical mode decomposition with adaptive noise. In: *Acoustics, Speech and Signal Processing (ICASSP), 2011 I.E. International Conference on, 2011. IEEE*, pp 4144–4147
- Trenberth KE, Hurrell JW (1994) Decadal atmosphere–ocean variations in the Pacific. *Clim Dyn* 9:303–319
- Trenberth KE, Shea DJ (2006) Atlantic hurricanes and natural variability in 2005. *Geophys Res Lett* 33:L12704
- Trenberth KE, Fasullo JT, Branstator G, Phillips AS (2014) Seasonal aspects of the recent pause in surface warming. *Nat Clim Chang* 4:911–916
- Watanabe M et al (2013) Strengthening of ocean heat uptake efficiency associated with the recent climate hiatus. *Geophys Res Lett* 40:3175–3179
- Wu Z, Huang NE, Wallace JM, Smoliak BV, Chen X (2011) On the time-varying trend in global-mean surface temperature. *Clim Dyn* 37:759–773
- Zhang R, Delworth TL, Held IM (2007) Can the Atlantic Ocean drive the observed multidecadal variability in Northern Hemisphere mean temperature? *Geophys Res Lett* 34(2):1944–8007